Available online at www.sciencedirect.com
ScienceDirect
International Journal of Mass Spectrometry 266 (2007) 166–179
International Journal of Mass Spectrometry
www.elsevier.com/locate/ijms

Collision-induced dissociation of fluoropyridinide anions

Shuji Kato*, W. Carl Lineberger, Veronica M. Bierbaum

Department of Chemistry and Biochemistry, University of Colorado and JILA, University of Colorado and National Institute of Standards and Technology, Boulder, CO 80309, USA

Received 2 May 2007; received in revised form 19 July 2007; accepted 19 July 2007
Available online 2 August 2007

Abstract

Collision-induced dissociation of *ortho*-fluoro, *meta*-fluoro, and 2,6-difluoropyridinide anions are studied using the selected ion flow tube technique. Structures and energetics of the reactants, transition states, and products are calculated at the MP4(SDQ)/6-31 + G(d) level of theory based on the B3LYP/6-311++G(d,p) and/or MP2/6-31 + G(d) optimized geometries. The monofluoropyridinide anions ($C_5NH_3F^-$) dissociate almost exclusively via loss of an HF molecule, i.e., $C_5NH_2^-$ + HF at low collision energies, in addition to loss of F^- at higher energies. 2,6-Difluoropyridinide anions ($C_5NH_2F_2^-$) dissociate via successive loss of HF molecules to form C_5NHF^- then C_5N^- depending on the collision energy. The CID results strongly suggest formation of ring-intact pyridynide structures ($C_5NH_2^-$, C_5NHF^-) with a bent triple bond embedded in the azine ring systems. Calculated reaction energy diagrams are totally consistent with the experimental observations. Didehydropyridynides $C_5NH_2^-$ and C_5NHF^- have substantial barriers to decomposition. Tetradehydropyridynide C_5N^- is a highly strained ring system and metastable with a predicted barrier of about 5 kcal mol^{-1} (20 kJ mol^{-1}) toward ring-opening to a linear NCCCCC$^-$ structure. The observed C_5N^- species is most likely the linear anion under experimental conditions; however, the ring-intact C_5N^- pyridynide is a highly energetic species releasing about 80 kcal mol^{-1} (340 kJ mol^{-1}) of energy upon the ring-opening.

Keywords: Collision-induced dissociation; Fluoropyridinide anion; Dehydropyridinide anion; High-energy density species; Molecular orbital calculation

1. Introduction

Didehydropyridines (pyridynes) are the smallest family of didehydroazines and reactive intermediates in solution phase chemistry [1]. Among the didehydropyridine structures, *ortho*-pyridynes (3,4-didehydropyridine **1** and 2,3-didehydropyridine **2**) have two adjacent hydrogen atoms abstracted from the pyridine substrate (Fig. 1). They are relatively stable but still strained and energetic because of the formally triple bond embedded in the six-membered ring system. Tetradehydropyridines with two formally triple bonds **3** and its isomer **4** are expected to be even more highly strained. Compared to the non-aza substituted analog of benzynes, the pronounced instability of pyridynes against unimolecular decomposition is due in part to the fact that the proximity of the nitrogen atom to the formally triple bond markedly decreases the thermodynamic stabilities [2]. When an aromatic ring system has more aza substitutions, lone-pair repulsions between the nitrogen atoms bring in additional instability, as demonstrated by a recent systematic theoretical study of Fabian and Lewars on polysubstituted azines (N0–N6) [3]. The N–N lone-pair repulsion appears to be the controlling factor whereas stabilization due to aromaticity is about the same across all azine members [3]. In fact, nitrogen lone-pair repulsion is a key design principle for pentazole (N_5)-based high energy density materials (HEDMs) [4–7]. The ring strain, nitrogen proximity to the triple bond, and lone-pair repulsions may be combined to devise an even more energetic class of HEDMs. Cioslowski et al. [2] theoretically investigated the energetics and electronic structures of didehydroazines with more than one nitrogen atom (up to N4). This paper also serves as an extensive list of previous theoretical studies on both benzynes and pyridynes.

In solution reactions, unambiguous verification of the didehydroazine intermediacy is challenging because other processes such as addition–elimination can lead to the same products as derived from the didehydro intermediates [1]. In the gas phase, photolysis of a precursor for 3,4-didehydropyridine **1** yielded a dimeric product which is suggestive of initial formation of the

* Corresponding author. Tel.: +1 303 492 7396; fax: +1 303 492 5894.
E-mail address: Shuji.Kato@colorado.edu (S. Kato).

1387-3806/$ – see front matter © 2007 Elsevier B.V. All rights reserved.
doi:10.1016/j.ijms.2007.07.016

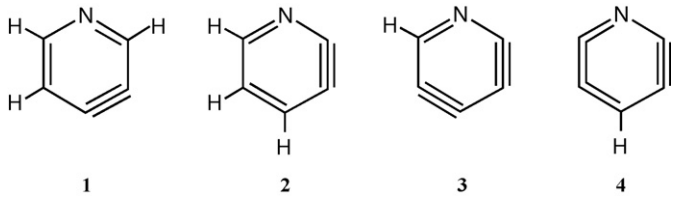

Fig. 1. Structures of didehydro- and tetradehydropyridines.

pyridyne [8]. The first direct evidence for the existence of **1** was obtained in a low-temperature matrix, in which a precursor for **1** was photolyzed and the pyridyne was spectroscopically identified [9]. An analogous attempt [10] to isolate **2**, which is about 25 kJ mol^{-1} higher in energy [2], failed however. For tetradehydropyridines **3** and **4** there is no experimental study and only a single theoretical paper is found in Ref. [11], which predicted both species to be stable at the CASSCF/3-21G level of theory with **4** being slightly lower in energy than **3** by 8 kJ mol^{-1}. An ionic analog of pyridyne ($C_5NH_3^{\bullet -}$ radical anion) has been suggested to be stable in the gas phase [12,13]. Following earlier work of Bruins et al. [12], Guo and Grabowski examined the reaction of the $O^{\bullet -}$ radical anion with pyridine [13]. Formal $H_2^{\bullet +}$ abstraction of benzene by $O^{\bullet -}$ produces the benzyne radical anion [12,14,15]. Based on the similarity of the rate constants and product branching ratios between the benzene and pyridine reactions, along with energetic discussions, they suggested that radical anions of pyridyne (**1**$^{\bullet -}$ and/or **2**$^{\bullet -}$) were formed from this reaction [13]. To our knowledge, however, essentially nothing is known experimentally or theoretically about the deprotonated analogs of pyridynes in the gas phase. In analogy to the deprotonated *ortho*-benzyne (2,3-dehydrophenyl anion) which is a highly delocalized structure around the formally triple bond [16], deprotonated forms of **1**–**4** are expected to be stable species and gas phase ion chemistry may provide a viable access to the exotic pyridyne structures.

In the present study, we investigate the collision-induced dissociation (CID) of *ortho*-fluoro-, *meta*-fluoro-, and 2,6-difluoropyridinide anions. For CID of non-aza substituted fluorophenyl anions, collisional excitation leads primarily to the loss of hydrogen fluoride molecule(s) and formation of deprotonated benzynide anions [16,17]. This observation is in sharp contrast to the CIDs of chlorophenyl [17,18] and bromophenyl anions [17]. CID of chlorophenyl anions proceeds via loss of Cl^- at low collision energy [18] and by electron detachment at high collision energy [17]. Loss of Br^- and electron detachment are the modes of dissociation for bromophenyl anions at high collision energy [17]. Indeed, chemical reactivity strongly suggests that heavier $C_6H_4X^-$ anions (X = Br, I) behave like halide–benzyne complexes, which easily transfer X^- to other neutral substrates [19,20]. We anticipate that the fluoropyridinide anions decompose in a manner similar to fluorophenyl anions, eliminating HF and possibly forming deprotonated pyridynide structures. We further note that in the CID of a difluorophenyl anion [16], successive elimination of two HF molecules produced the C_6H^- species. Although the C_6H^- structure is yet to be identified, a ring-intact form of C_6H^- is a highly strained compound that can release an enormous amount of energy upon ring-opening to the more stable linear C_6H^- structure (Kato et al., unpublished results). By analogy, CID of 2,6-difluoropyridinide might produce the C_5N^- anion, either in the deprotonated form of **3** or **4** or a linear structure. We examine product distributions from CID of the fluoropyridinide anions as a function of the collision energy. Molecular orbital calculations are conducted to discuss the CID pathways including formation of ring-intact pyridynide versus ring-opened chain anions.

2. Experimental methods

Collision-induced dissociation experiments were conducted using a flowing afterglow–selected ion flow tube (FA–SIFT), which has been described previously [21–23]. Deprotonated fluoropyridinide anions (*o*-$C_5NH_3F^-$, *m*-$C_5NH_3F^-$, 2,6-$C_5NH_2F_2^-$) were prepared in the source flow tube by deprotonation of the parent fluoropyridines by hydroxide anions in a flow of helium buffer gas (≅40 Pa). The $[M-H]^-$ ions were extracted into the quadrupole mass filter region, mass selected, and injected into the second flow tube containing helium (≅65 Pa and 300 K). Collision with helium takes place in the vicinity of the injection orifice (i.e., SIFT–CID) that connects the quadrupole region and the second flow tube. The injection energy (E_{lab}), defined as the voltage difference between the source flow tube and the injection orifice, was adjusted from 20 to 80 eV to explore different collision energies between the ion and the helium buffer gas [24,25]. The ionic fragmentation products as well as the $[M-H]^-$ ions were detected at the end of the second flow tube using a quadrupole mass spectrometer.

It should be noted that under these high-pressure SIFT–CID conditions all ions undergo collision and multiple collision events are possible. Nominal center-of-mass collision energies (E_{cm}) can be calculated using the relation $E_{cm} = E_{lab} \cdot m_{He}/(m_{He} + m_{ion})$, where m_{He} and m_{ion} are the masses of He and the reactant ion, respectively. In SIFT–CID, however, large molecular ions such as these tend to accumulate internal energy more effectively from multiple collisions thereby decomposing at artificially lower threshold energies. The E_{cm} should thus be taken as the lower bound for the actual internal excitation of the anions. All experiments from different precursor ions were conducted back-to-back in order to eliminate potential problems due to slight drifts in the CID and ion detection conditions. Mass discrimination between ions of different masses was minimized by tuning the detection with standard anions, and no further corrections were made in the analysis.

3. Quantum chemical calculations

Geometry optimizations and frequency calculations were carried out with the density functional B3LYP method using the 6-311++G(d,p) basis set within the Gaussian03 suite of programs [26]. Transition states connecting two local minima were identified from animation of the single imaginary frequency. Intrinsic reaction coordinate (IRC) calculations were also employed to confirm some of the minima connected by the given transition state [27,28]. In order to optimize the accuracy of the

present calculations with specific requirements (calculation of transition state energies, treatment of electron correlation involving F atoms [29], and some biradical character [30]), single point electronic energies were calculated using the MP4(SDQ)/6-31 + G(d) level of theory on each of the B3LYP stationary point geometries. For a similar system of *o*-benzyne and its deprotonated anion, the MP4(SDQ)/6-31 + G(d) approach is found to produce results that are consistent with calculations using very high level of theory at CCSD(T)/aug-cc-pVTZ (Kato et al., unpublished results). The B3LYP frequency calculations provided zero point energy (ZPE) and thermal corrections to the MP4 electronic energy. For some critical and/or important stationary points, geometries and frequencies were also calculated by full ab initio methods using the more demanding MP2/6-31 + G(d) computations. MP4(SDQ)/6-31 + G(d) single point calculations were similarly performed on the MP2 optimized geometries. MP2/6-31 + G(d) alone was found to give unpredictably erratic results in the electronic energy part of the calculation, a trend also confirmed by comparing the MP2 results with CCSD(T)/aug-cc-pVTZ computations (Kato et al., unpublished results). No scaling factor was applied to the calculated vibrational frequencies.

Computational results were inter-compared among the three levels of theory employed, i.e., B3LYP/6-311++G(d,p), MP4(SDQ)/6-31 + G(d)//B3LYP/6-311++G(d,p), and MP4(SDQ)/6-31 + G(d)//MP2/6-31 + G(d). Calculated deprotonation enthalpies ($\Delta_{acid}H_{298}$) are in excellent agreement within 5 kJ mol^{-1} in most cases. As anticipated, however, the full B3LYP computations produced some erratic results elsewhere. Therefore, in the present study, all energies are reported at MP4(SDQ)/6-31 + G(d)//B3LYP/6-311++G(d,p) unless otherwise specified, in terms of standard enthalpies at 298 K (ΔH_{298}). The only exception is an empirical adjustment to the calculated energies for hydrogen fluoride and the fluoride anion; the MP4(SDQ)/6-31 + G(d) computations with the relatively small basis set are found to overestimate the hydrogen fluoride energy while underestimating the F^- energy, thus predicting an anomalously small value for the deprotonation enthalpy $\Delta_{acid}H_{298}$(HF) as compared to the very accurate experimental value of 1554 kJ mol^{-1} [31]. The adjustment is made based on the observation that calculated heats of formation for HF and F^- asymptotically approach the experimental values at the large basis set limit so that they reproduce the experimental $\Delta_{acid}H_{298}$(HF). The corrected HF and F^- enthalpies are used to construct the potential energy diagrams for CID.

4. Results

4.1. Gas phase acidities of fluoropyridines

Fig. 2 shows the calculated deprotonation enthalpies ($\Delta_{acid}H_{298}$) for *o*-fluoro, *m*-fluoro, and 2,6-difluoropyridines. The B3LYP and MP4(SDQ)//B3LYP theories predict acidity values that are mutually consistent. Although experimental acidity values are unknown for these species, the calculations suggest that the fluoropyridines have multiple acidic sites in the molecule. *o*-Fluoropyridine has three acidic hydrogens that

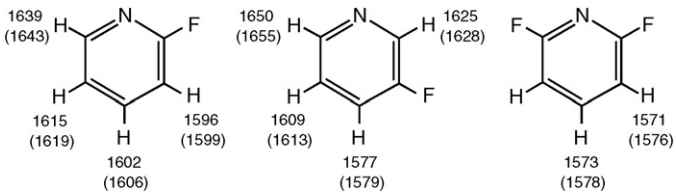

Fig. 2. *ortho*-Fluoro, *meta*-fluoro, and 2,6-difluoropyridines and site-specific heats of deprotonation ($\Delta_{acid}H_{298}$ in kJ mol^{-1}) calculated at MP4(SDQ)/6-31 + G(d)//B3LYP/6-311++G(d,p). Values in parentheses indicate heats of deprotonation at B3LYP/6-311++G(d,p).

can be deprotonated by HO^- ($\Delta_{acid}H_{298}$ = 1633 kJ mol^{-1}). The C3 and C4 positions are the most acidic with their deprotonation enthalpies differing only slightly. *m*-Fluoropyridine also has three acidic hydrogens that are accessible by HO^-. The C4 position is considerably more acidic than the others. For 2,6-difluoropyridine the C3 and C5 sites are identical by symmetry and highly acidic; these positions are marginally more acidic than the C4 position. All these acidic sites may be deprotonated to yield the corresponding $[M - H]^-$ anions. It should be noted that, under the high-pressure conditions in the SIFT source flow tube, nascent $[M - H]^-$ ions may undergo self-quenching collisions with the precursor pyridine molecules to isomerize to the more stable structures [32]. In the following sections, however, all possible isomers will be considered.

4.2. CID of ortho- and meta-fluoropyridinide anions

Following CID of *o*- and *m*-fluoropyridinide anions, good agreement was observed between the depletion of the $[M - H]^-$ reactants and the summed formation of the products, suggesting that electron detachment of the reactant or product ions is negligible. Tables 1 and 2 show the relative abundances of observed ionic species normalized to 100% for each of the collision energies. Noticeable differences as well as similarities are observed between the CID products of *o*- and *m*-fluoropyridinide anions (Tables 1 and 2). Both reactant anions (*m*/*z* 96) eliminate HF to form $C_5NH_2^-$ species at *m*/*z* 76, presumably ring-intact pyridynide anions. The yields of F^- (*m*/*z* 19), a product that may arise from C–F bond rupture of the precursor anions, are small compared to $C_5NH_2^-$. Other products commonly observed from the two reactants are HC_2^- (*m*/*z* 25), CN^- (*m*/*z* 26), and C_3N^- (*m*/*z* 50), whereas HC_4^- (*m*/*z* 49) and HC_4^-·HF (*m*/*z* 69) are observed only from *m*-fluoropyridinide. It can be seen that *m*-fluoropyridinide is more susceptible to dissociation.

Collision energy dependences of the product yields (Tables 1 and 2) indicate that HF elimination is the lowest energy process; F^- elimination was not observed at the lowest injection energy of E_{lab} = 20 eV. A difference was observed in the relative abundances of $C_5NH_2^-$ versus F^- for the *o*- and *m*-pyridinide anions; *o*-pyridinide produces a relatively large amount of F^- and a small amount of $C_5NH_2^-$ as compared to *m*-pyridinide. For both reactants the F^- yield increases steadily with the increase in the collision energy, whereas the $C_5NH_2^-$ yield maximizes at 50 eV before decreasing at 70 eV. This suggests that the nascent $C_5NH_2^-$ species fragment and/or other

Table 1
The normalized SIFT-CID mass spectra of the *ortho*-$C_5NH_3F^-$ anion as a function of the collision energy

E_{lab} (eV)	E_{cm} [a] (eV)	*m/z* 96 (o-$C_5NH_3F^-$)	*m/z* 76 ($C_5NH_2^-$)	*m/z* 69 (HC_4^-·HF)	*m/z* 50 (C_3N^-)	*m/z* 49 (HC_4^-)	*m/z* 26 (CN^-)	*m/z* 25 (HC_2^-)	*m/z* 19 (F^-)
20	0.8	92.6	4.9	–[b]	2.5	–	–	–	–
35	1.4	77.6	7.8	–	8.6	–	2.6	–	3.4
50	2.0	37.6	20.4	–	21.0	–	8.0	2.5	10.5
70	2.8	7.6	12.0	–	40.4	–	12.0	7.8	20.2

[a] Nominal center-of-mass collision energy.
[b] Indicates that signal could not be discerned above the noise.

Table 2
The normalized SIFT-CID mass spectra of the *meta*-$C_5NH_3F^-$ anion as a function of the collision energy

E_{lab} (eV)	E_{cm} [a] (eV)	*m/z* 96 (m-$C_5NH_3F^-$)	*m/z* 76 ($C_5NH_2^-$)	*m/z* 69 (HC_4^-·HF)	*m/z* 50 (C_3N^-)	*m/z* 49 (HC_4^-)	*m/z* 26 (CN^-)	*m/z* 25 (HC_2^-)	*m/z* 19 (F^-)
20	0.8	89.4	6.1	–[b]	4.5	–	–	–	–
35	1.4	64.0	17.6	–	8.0	–	4.0	0.8	5.6
50	2.0	18.9	37.2	1.6	19.9	3.1	7.3	2.6	9.4
70	2.8	1.2	17.6	2.1	34.0	7.3	14.8	10.6	12.4

[a] Nominal center-of-mass collision energy.
[b] Indicates that signal could not be discerned above the noise.

dissociation channels become accessible at higher levels of collisional excitation. The smaller product ions HC_2^-, CN^-, and C_3N^- are indicative of the occurrence of these processes that are competitive at higher collision energies.

4.3. CID of 2,6-difluoropyridinide anion

Table 3 shows the normalized yields of the reactant and product ions in the CID of 2,6-difluoropyridinide. Electron detachment appears to be negligible since the sum of the ion intensities remains approximately constant. Fig. 3 is the mass spectrum at E_{lab} = 80 eV and Fig. 4 shows the CID energy dependence of the major ionic species.

Given the similar ranges of E_{cm} explored, the difluoropyridinide anion is found to fragment less easily than the *o*- and *m*-fluoropyridinide anions. The reactant anion (*m/z* 114) eliminates HF to form the C_5NHF^- species (*m/z* 94), a potential fluorinated analog of the ring-intact pyridynide anion. Fluoride was not observed at the lowest collision energy of E_{lab} = 20 eV, where C_5NHF^- is the only CID product. Overall, F^- is a relatively minor product compared to the CID spectra of *o*- and *m*-fluoropyridinide anions; the F^- formation starts

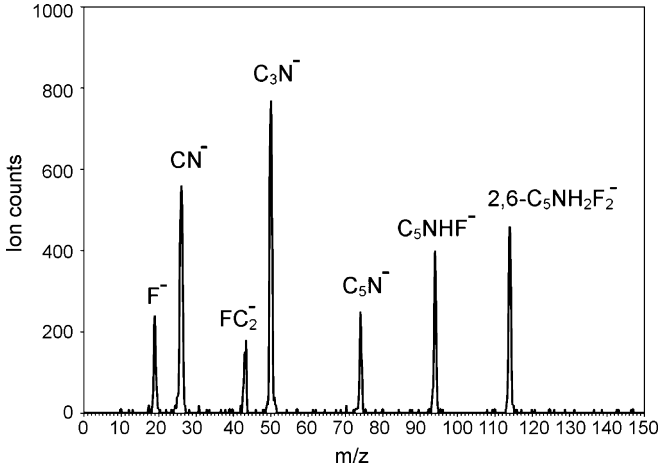

Fig. 3. CID mass spectrum of 2,6-difluoropyridinide anion at E_{lab} = 80 eV.

to be competitive only at the highest collision energy examined ($E_{lab} \approx 80$ eV). The C_5NHF^- yield peaks at 70 eV then decreases at 80 eV, suggesting fragmentation of the primary species and/or loss of another HF molecule to form C_5N^- (*m/z* 74) as observed. Major fragment anions are C_3N^- (*m/z* 50)

Table 3
The normalized SIFT-CID mass spectra of the 2,6-$C_5NH_2F_2^-$ anion as a function of the collision energy

E_{lab} (eV)	E_{cm} [a] (eV)	*m/z* 114 ($C_5NH_2F_2^-$)	*m/z* 94 (C_5NHF^-)	*m/z* 74 (C_5N^-)	*m/z* 50 (C_3N^-)	*m/z* 49 (HC_4^-)	*m/z* 43 (FC_2^-)	*m/z* 26 (CN^-)	*m/z* 25 (HC_2^-)	*m/z* 19 (F^-)
20	0.7	99.3	0.7	–[b]	–	–	–	–	–	–
50	1.7	86.7	7.1	1.1	2.8	–	–	1.7	–	0.6
60	2.0	66.9	11.9	1.8	8.2	–	0.9	7.9	–	2.4
70	2.4	39.6	16.9	3.8	18.8	–	3.1	11.9	0.9	5.0
80	2.7	15.7	13.7	8.5	26.3	1.0	6.1	19.1	1.4	8.2

[a] Nominal center-of-mass collision energy.
[b] Indicates that signal could not be discerned above the noise.

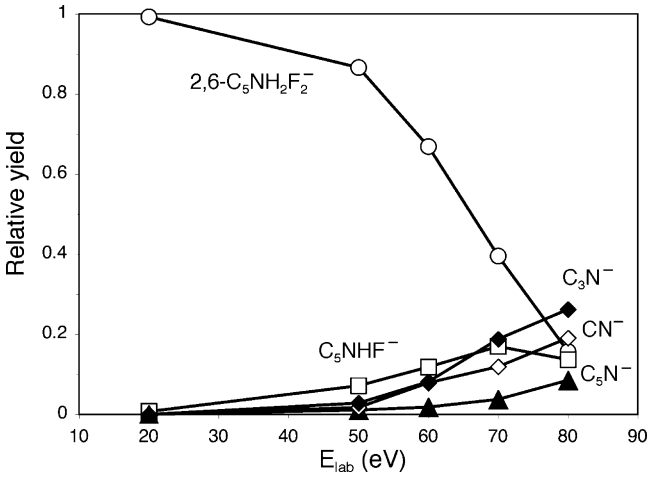

Fig. 4. Collision energy (E_{lab}) dependence of the relative yields for 2,6-difluoropyridinide anion and the major CID products taken from Table 3. The yield of F^- is almost identical to that of C_5N^-.

and CN^- (*m*/*z* 26) while the yield of HC_2^- (*m*/*z* 25) is significantly small compared to the CID of monofluoropyridinide anions. Instead, FC_2^- (*m*/*z* 43) is a characteristic product from dissociation of the difluoropyridinide.

5. Discussion

5.1. General CID schemes

The product distributions from CID of the fluoropyridinide anions suggest that several dissociation pathways are accessed, (i) competitive elimination of HF versus F^- from $[M-H]^-$ as also observed in the CID of the fluorophenyl anion [16], (ii) fragmentation of the primary product anion $[M-H-HF]^-$, and (iii) ring-opening of the $[M-H-HF]^-$ anion when it is an intact pyridynide structure. Prior to quantitative discussions of individual reactions, it is useful to summarize general schemes that have been computationally identified.

Consider the CID of *m*-fluoropyridine-4-anion (Scheme 1). Upon collisional excitation, release of F^- is the lowest energy path within the dissociating complex. Analogous to the CID of fluorophenyl anion [16], F^- may directly leave the complex (1a) or abstract the adjacent hydrogen atom before exiting as HF (1b). The fluoride anion cannot migrate in the pyridyne plane beyond the nitrogen atom or the formally triple bond (as schematically shown by the broken lines of prohibited access) because of the in-plane lone-pair/π-lobe repulsions. In fact, MP4(SDQ)/6-31 + G(d) calculations indicate that potential energies for F^- are always repulsive along these lines towards the infinite separation of F^-. Alternatively, F^- may move over or under the *ortho*-pyridyne plane and attaches to either of the two hydrogen atoms (H′) on the other side of the ring (1c). This will lead to elimination of H′F as well as of F^- (shown in parentheses). Existence of such "crossover" transition states has been demonstrated both experimentally and computationally [33,34].

Within the activated complex of the *o*-fluoropyridine-3-anion (Scheme 2), the F^- species cannot migrate in the *ortho*-pyridyne plane because of the repulsive potential energy walls. The fluoride anion either leaves the complex (2a) or migrates to the other side of the complex via the crossover transition state (2b).

In collisional excitation of the *o*-fluoropyridinide 4-anion (Scheme 3), release of F^- will lead to the formation of an intermediate involving 2,4-*meta*-pyridyne. F^- may directly leave the complex (3a) or migrate in the plane of the complex before abstracting either of the hydrogen atoms (3b). No repulsive barrier is located computationally for F^- migrating across these radical sites.

Following elimination of HF, the deprotonated pyridyne structures may remain intact or ring-open depending on the stabilities and levels of internal excitation. Ring-opening of pyridynide anions (Scheme 4) is found to proceed analogously to benzynide decomposition; detailed discussions of the ring-opening mechanisms will be given elsewhere (Kato et al., unpublished results). If the formal anionic charge is located β to the formally triple bond (4a), the pyridynide ring-opens via a transition state that connects to a stable acetylide structure. If the formal anionic charge is located α to the formally triple bond (4b), the ring-opening begins as if it were to generate a vinyl species. The vinyl structure, however, is unstable and further rearranges on its way to the transition state that resembles an ensemble of fragmented products. These mechanisms apply to ring-opening of all pyridynide anions in the present study except for 2,3-didehydro-4-anions which have significantly distorted structures (**12** in Fig. 7 and **31** in Fig. 11, see below) and the 3,4-didehydro-2-anion (**33** in Fig. 11, see below) for which

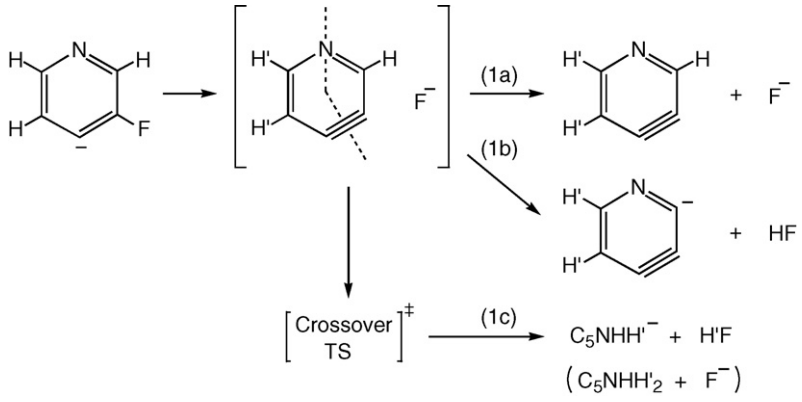

Scheme 1. CID of *meta*-fluoropyridine-4-anion.

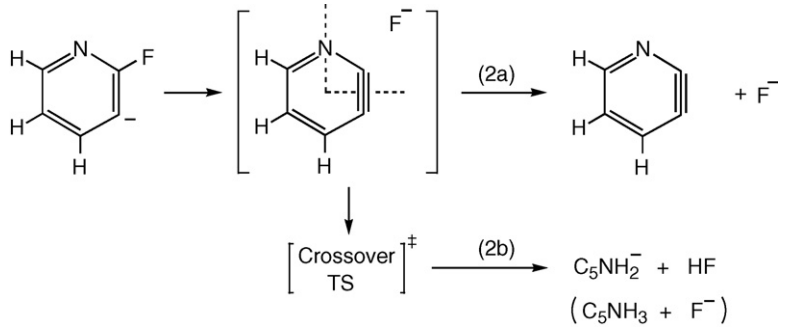

Scheme 2. CID of *ortho*-fluoropyridine-3-anion.

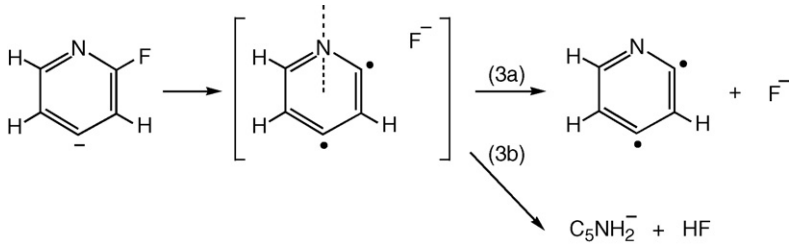

Scheme 3. CID of *ortho*-fluoropyridine-4-anion.

the vinyl structures are stabilized by the fluorine atom at both the transition state and product.

Molecular motions along the intrinsic reaction coordinate are consistent with the crossover (1c and 2b) and ring-opened (4a) transition states connecting the respective minima, although completion of IRC calculations is found difficult for the crossover transition states presumably because of the very flat potentials around the transition states.

Triplet states were also calculated at MP4(SDQ)/6-31 + G(d)//B3LYP/6-311++G(d,p) for pyridyne-type (**1**, **2**, **6**, **14**, **15**, **26**, **27**, and **29**) and cumulene-type (**16** and **28**) structures to explore the possibility that some of the low-lying states may provide an alternative surface for decomposition. Triplet states for the *o*- and *m*-pyridyne-type structures are significantly higher in energy than the corresponding singlet states; the values for singlet–triplet splitting (electronic + ZPE) are 133, 79, and 76 kJ mol^{-1} for *o*-pyridyne structures **1**, **2**, and **26**, respectively, and 309 and 114 kJ mol^{-1} for *m*-pyridyne structures **6** and **29**, respectively (**14** has failed convergence at MP4). *p*-Pyridyne structures have relatively low triplet states with singlet–triplet splitting of 14 and 4 kJ mol^{-1} for **15** and **27**, respectively, but the triplet states for the corresponding retro-Bergman ring-opened products **16** and **28** are both higher than the singlet by 236 kJ mol^{-1}. In the following discussion, only singlet surfaces will be considered for the dissociation pathways.

5.2. CID mechanisms of monofluoropyridinide anions

Figs. 5 and 6 display structures and relative energies of species associated with unimolecular decompositions of *meta*- and *ortho*-fluoropyridinide anions, respectively. To highlight the relative stabilities of the species involved, energies ($\Delta_{298}H$) are referenced to the most stable structure in each family of the reactants, neutral intermediate structures, and products. Following initial release of F^- within the complex, the most stable *m*-fluoropyridinide-4-anion (≡0 kJ mol^{-1}) forms a [pyridyne + F^-] intermediate of 3,4-didehydropyridine **1** (Fig. 5). Proton abstraction of F^- within the intermediate leads immediately to the formation of **9**. Alternatively, a passage of F^- over the crossover transition state **TS1** (235 kJ mol^{-1} higher in energy than the reactant, with the F^- species located ca. 2.9 Å above the pyridyne plane) facilitates formation of **7** and **8**. The higher-

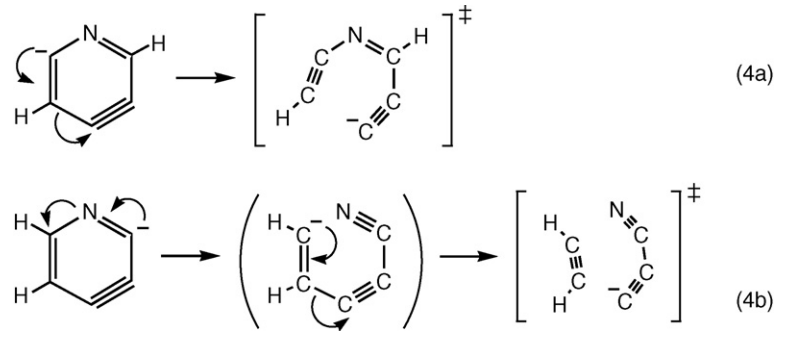

Scheme 4. Typical mechanisms and transition state structures for ring-opening of pyridynide anions.

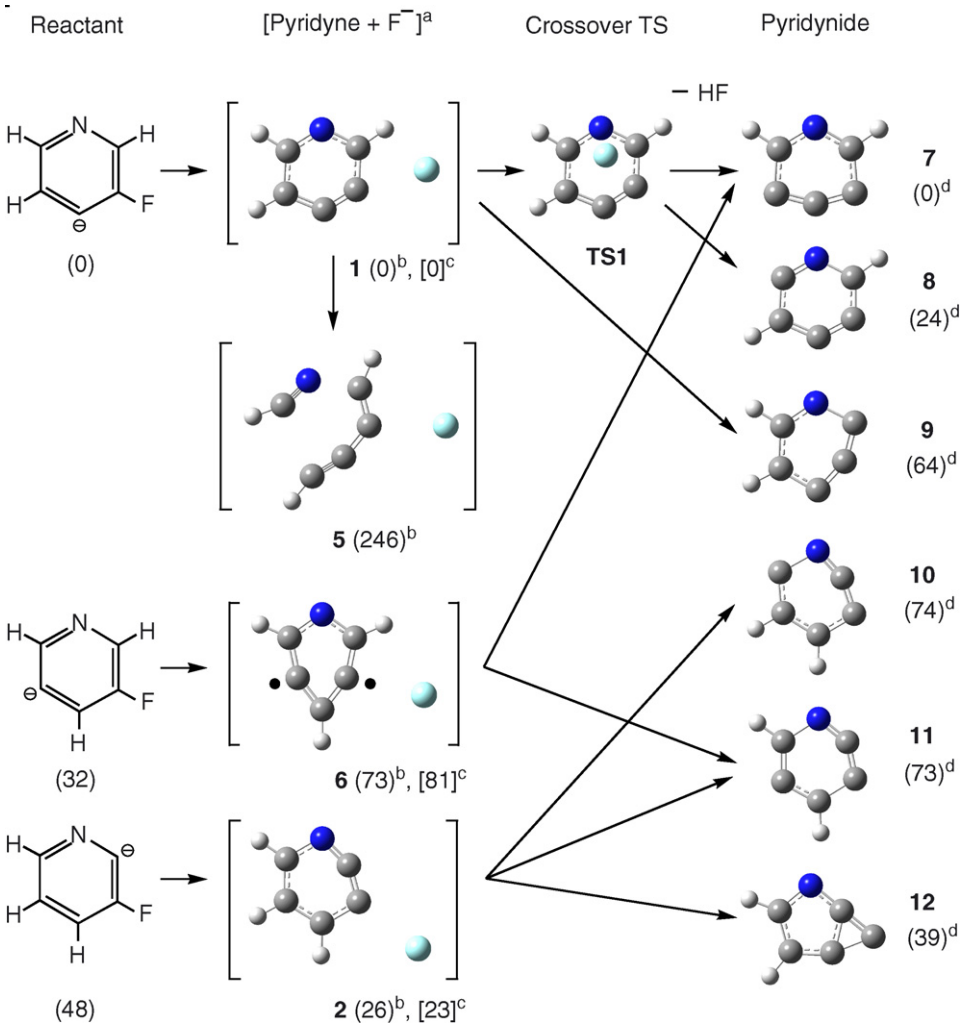

Fig. 5. Relative energies $\Delta_{298}H$ (electronic + ZEP + thermal correction) in kJ mol^{-1} calculated for the decomposition of *m*-fluoropyridinide anions at MP4(SDQ)/6-31 + G(d)//B3LYP/6-311++G(d,p). [a]Energies for isolated neutral C_5NH_3 structures are indicated. Positions of the F^- species are schematically shown; [b]Energies relative to **1**. [c]Energies relative to **1** at CCSD(T)/cc-pVTZ [2]. [d]Energies relative to **7**.

energy 5-anion (32 kJ mol^{-1}) initially forms a [pyridyne + F^-] intermediate of 3,5-didehydropyridine **6**, which is significantly higher in energy than **1**. The 2-anion (48 kJ mol^{-1}) forms a [pyridyne + F^-] intermediate of 2,3-didehydropyridine **2**. These higher-energy intermediates correlate with formation of **10**–**12** in addition to **7**. It is noted that the MP4(SDQ)/6-31 + G(d) relative energies for pyridynes (**1**, **2**, **6** and also **14** in Fig. 6) are in excellent agreement with those calculated at a higher level using CCSD(T)/cc-pVTZ [2]. The MP4(SDQ)/6-31 + G(d) relative energy of 2,3-*ortho*-pyridyne **2** is 26 kJ mol^{-1} higher than 3,4-*ortho*-pyridyne **1** for both the B3LYP/6-311++G(d,p) and MP2/6-31 + G(d) optimized geometries.

The neutral pyridyne **1** may also decompose within the complex in a concerted retro-Diels–Alder fashion to form **5**. With the approximation that F^- is a spectator, the decomposition requires an additional energy of 246 kJ mol^{-1} above the energy of **1**. It has been demonstrated from experiments and high-level computations that retro-Diels–Alder is the principal mode of decomposition for *o*-benzyne [35]. The MP4(SDQ)/6-31 + G(d) level of theory predicts the 0 K transition-state barrier for *o*-benzyne to be 387 and 386 kJ mol^{-1} for optimized geometries of MP2/6-31 + G(d) and B3LYP/6-311++G(d,p), respectively. These TS energies are in good agreement with the CCSD(T)-AE/cc-pCVQZ value [35] of 368 kJ mol^{-1} (the MP2 geometry optimization produced a single imaginary frequency of 434 *i* cm^{-1} whereas the B3LYP optimization returned a saddle point of the second order with imaginary frequencies of 563 *i* and 101 *i* cm^{-1}, as similarly observed in the B3LYP computations of Moskaleva et al. [36]). The MP4//MP2 and MP4//B3LYP product energies (0 K) for HCCCCH + HCCH (200 and 213 kJ mol^{-1}, respectively) also compare well with that of CCSD(T)-AE/cc-pCVQZ (219 kJ mol^{-1}) [35]. These agreements provide support for the levels of theory used and the semi-quantitative discussions in the present study.

In HF elimination of the *o*-fluoropyridinide anions (Fig. 6), the most stable *o*-fluoropyridinide-3-anion (≡0 kJ mol^{-1}) initially forms a [pyridyne + F^-] intermediate of 2,3-didehydropyridine **2**. Because no hydrogen atom is immediately available, the F^- species must crossover to the other side of the ring via **TS2** (259 kJ mol^{-1} higher in energy than the

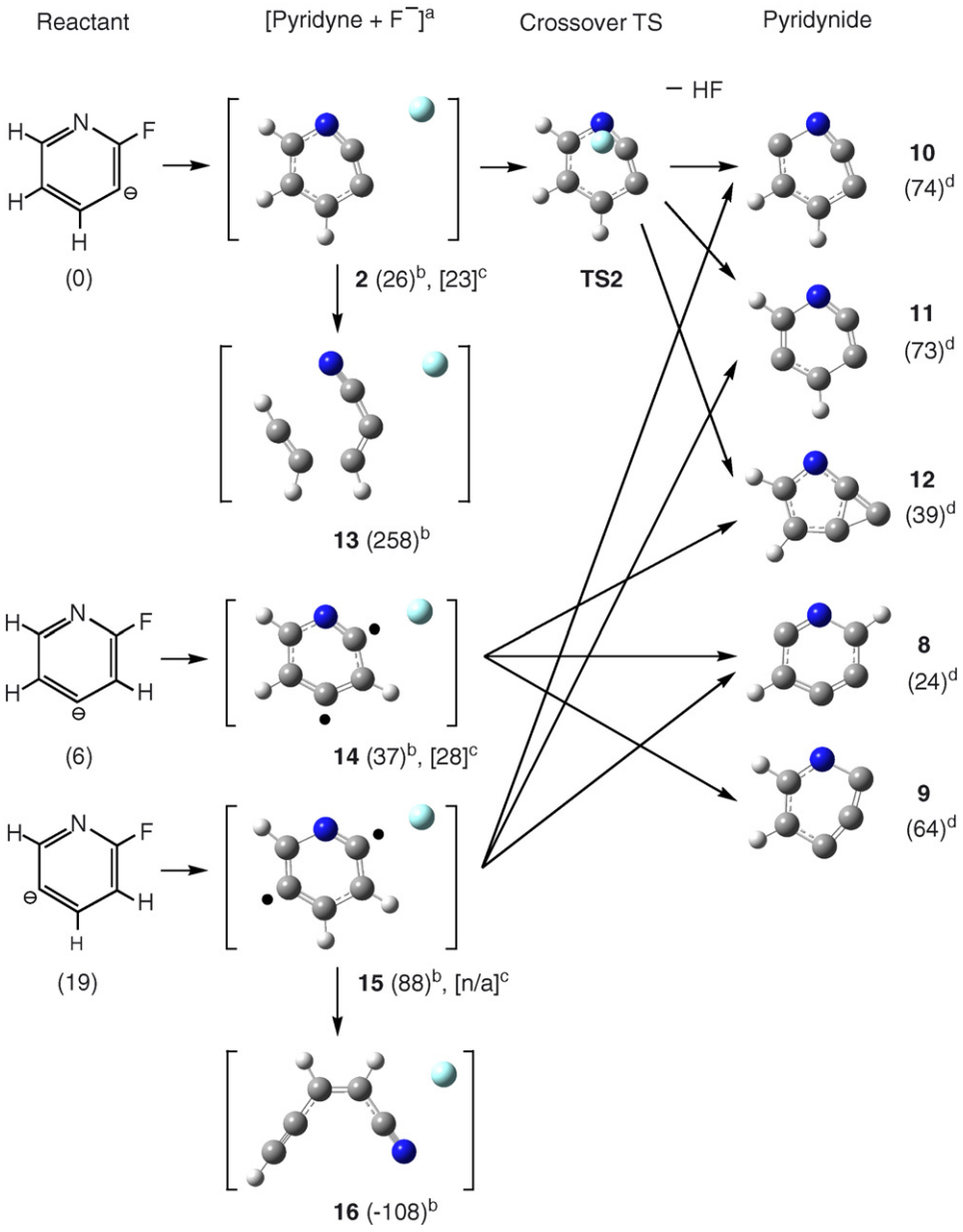

Fig. 6. Relative energies $\Delta_{298}H$ (electronic + ZEP + thermal correction) in kJ mol^{-1} calculated for the decomposition of *o*-fluoropyridinide anions at MP4(SDQ)/6-31+G(d)//B3LYP/6-311++G(d,p). [a]Energies for isolated neutral C_5NH_3 structures are indicated. Positions of the F^- species are schematically shown; [b]Energies relative to **1**. [c]Energies relative to **1** at CCSD(T)/cc-pVTZ [2]. [d]Energies relative to **7**.

reactant, with the F^- species located ca. 2.8 Å above the pyridyne plane) to produce **10**, **11**, or **12**. Retro-Diels–Alder decomposition of **2** to form **13** requires a substantial amount of additional excitation (232 kJ mol^{-1}) above the energy of **2**. The 4-anion (6 kJ mol^{-1}) initially forms a [pyridyne + F^-] intermediate of 2,4-didehydropyridine **14** while the 5-anion (19 kJ mol^{-1}) forms 2,5-didehydropyridine **15** within the complex. The *meta*-pyridyne **14** intermediate affords additional pathways for products **8** and **9**, while the *para*-pyridyne structure **15** is more likely to undergo facile retro-Bergman ring-opening [2,37,38] to **16**; the *para*-pyridyne is only stable at the B3LYP level, as shown here and elsewhere [2], and at CASSCF and CASMP2 [38] but ring-opens at a higher level of theory with CCSD(T)/cc-pVTZ [2]. Site-specific deprotonation enthalpies for **16**, i.e., $H^{(1)}C{\equiv}CCH^{(2)}{=}CH^{(3)}C{\equiv}N$ are calculated at MP4(SDQ)/6-31 + G(d)// B3LYP/6-311++G(d,p) to be $\Delta_{acid}H_{298}$ = 1502, 1538, and 1536 kJ mol^{-1} for $H^{(1)}$, $H^{(2)}$, and $H^{(3)}$, respectively. F^- deprotonation of $H^{(1)}$ or $H^{(3)}$ yields anions of similar (Z) structures, whereas $H^{(2)}$ deprotonation forms an (E) anion following a significant conformational change around the formally double bond. This is the only mechanism for HF elimination of monofluoropyridinide anions *without* forming the pyridynide structures.

Fig. 7 summarizes structures and energetics associated with ring-opened transition states and products from CID of *o*- and *m*-fluoropyridinide anions. Energies ($\Delta_{298}H$) are referenced to the pyridynide anions **7**–**12**. Anions **8**–**12** are commonly derived from *o*- and *m*-fluoropyridinides whereas formation of **7** is spe-

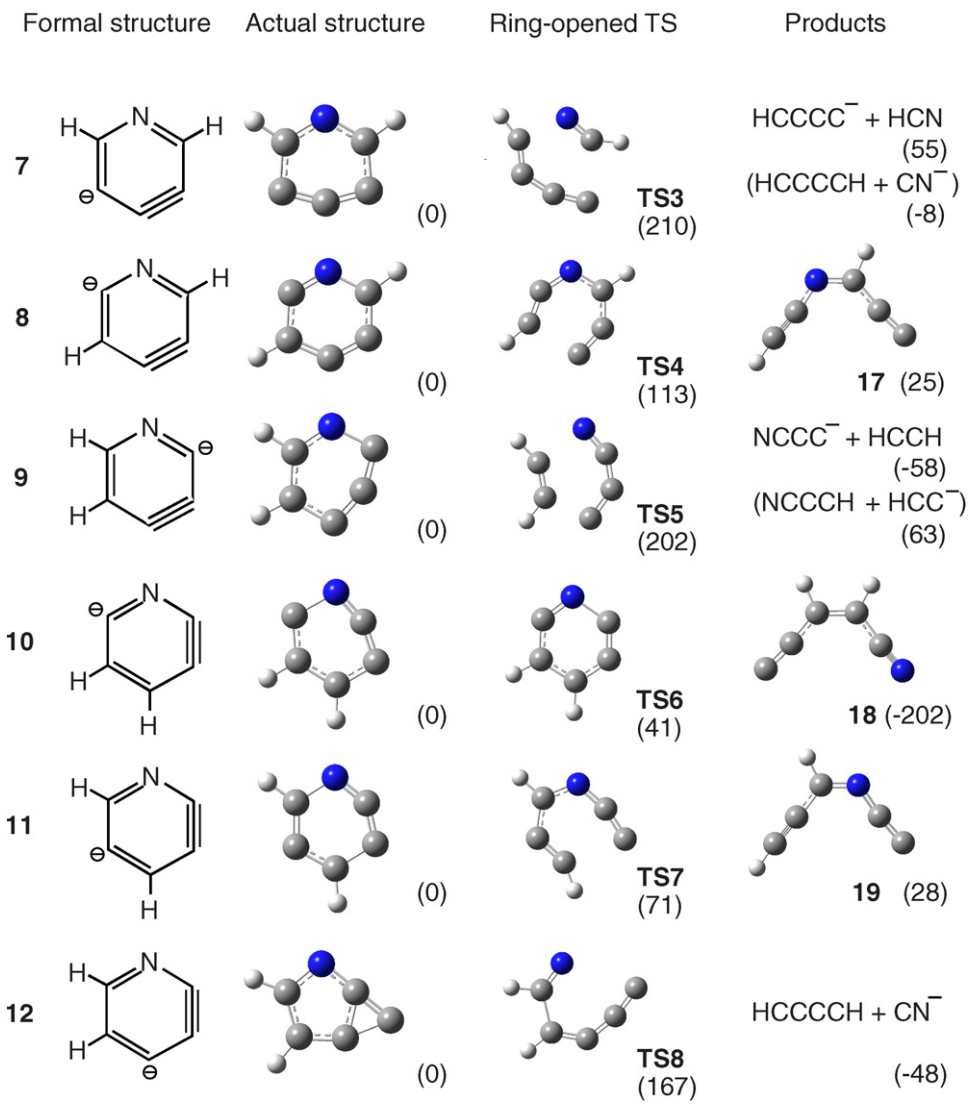

Fig. 7. Relative energies $\Delta_{298}H$ (electronic + ZEP + thermal correction) in kJ mol^{-1} calculated for ring-opening of the pyridynide anions at MP4(SDQ)/6-31 + G(d)//B3LYP/6-311++G(d,p). All energies are relative to each of the pyridynide structures.

cific to *m*-fluoropyridinide. Adiabatic electron binding energies (electronic + ZPE) are calculated at B3LYP/6-311++G(d,p) to be 2.53 (**7**), 2.24 (**8**), 1.66 (**9**), 2.12 (**10**), 2.33 (**11**), and 1.70 eV (**12**). Pyridynide anions with the formal anionic charge β to the formally triple bond (**8**, **10**, and **11**) form stable acetylide anions (**17**–**19**, respectively) via transition states that are relatively low in energy. In particular, decomposition of **10** with the lowest barrier and largest exothermicity involves an early transition state **TS6**, whose structure resembles the reactant. Compared to the β-anions, α-anionic pyridynide anions (**7** and **9**) have considerably higher transition states, in which they have essentially fragmented. Repulsive dynamics of $HCCCC^-$ and HCN (532 $i\,cm^{-1}$) at **TS3** may allow for direct dissociation to $HCCCC^-$ + HCN in competition with the formation of a more stable product pair $HCCCCH + CN^-$, in analogy to the direct product dynamics of an S_N2 reaction [39]. An intriguing exception to the ring-opening schemes is the decomposition of **12**, which involves a C–N bond cleavage at **TS8**. Further, the ensuing chain product anion is computationally found to be unstable; following the transition state, the anion liberates hydrogen cyanide and rearranges to a linear structure [$HCCCC^-\cdots$HCN]. This adduct is likely to separate as a more stable proton-transferred pair of $HCCCCH + CN^-$.

Figs. 8 and 9 show the potential energy diagrams for CIDs of *m*-fluoro and *o*-fluoropyridinides, respectively. The diagrams have been constructed for reactant anions that are likely accessible under thermal-energy flow tube conditions. The computational results are consistent with the experiments that HF elimination is the lowest dissociation channel observed. For both *m*- and *o*-pyridinides, crossover transition states (**TS1** and **TS2**) are lower in energy than the F^- elimination channels. The F^- species then attaches to one of the hydrogen atoms to form stable adducts (**20**–**22** and **23**–**25**). It can be seen that these adducts are precursors to HF elimination with elongated C–H bonds; they can also lose F^- competitively. Elimination of HF from these adducts appears to be direct since no transition states or local minima are found on the way to dissociation to pyridynides **7**–**9** and **10**–**12**. Several of these pathways (**7**, **8**, **12**) are lower in

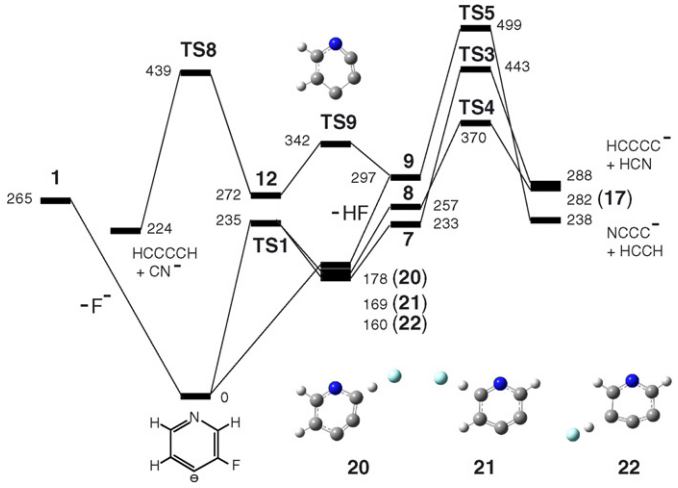

Fig. 8. Reaction energy diagram for the decomposition of *m*-fluoropyridinide anion. The relative energies $\Delta_{298}H$ (electronic + ZPE + thermal correction) are calculated at MP4(SDQ)/6-31 + G(d)//B3LYP/6-311++G(d,p) and shown in kJ mol^{-1}.

energy than the F^- channels, substantiating that HF elimination is the lowest energy path available.

The crossover transition state, pyridynide product, and F^- channel are all lower in energy for *m*-pyridinide than for *o*-pyridinide. This is also consistent with the experimental observation that the *m*-anion is more susceptible to CID. It is interesting to note that the CID of *o*-pyridinide produces somewhat more F^- than the CID of *m*-pyridinide. Relative energetics between HF and F^- eliminations are similar for *o*- and *m*-anion CIDs and do not seem to account for the observed difference. The *m*-anion can directly form adduct **20** without the need to surmount the crossover barrier; however, the adduct is energetically better correlated with formation of F^- than of HF and **9**. The most important aspect in the CIDs of monofluoro pyridinides

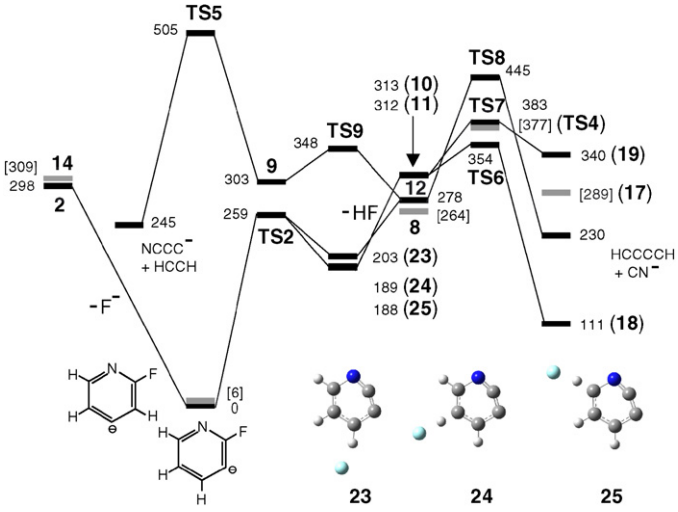

Fig. 9. Reaction energy diagram for the decomposition of *o*-fluoropyridinide-3-anion. Energy levels for *o*-fluoropyridinide-4-anion are also indicated in grey with the energy values in square brackets. The relative energies $\Delta_{298}H$ (electronic + ZPE + thermal correction) are calculated at MP4(SDQ)/6-31 + G(d)//B3LYP/6-311++G(d,p) and shown in kJ mol^{-1}.

is that there are substantial barriers to secondary decomposition of the nascent pyridynide anions. The ring-opened transition states (**TS3**–**TS8**) are all significantly higher in energy than the F^- channels. When there is no F^- elimination observed at low collision energies, the [pyridinide – HF]$^-$ products must be intact pyridynide structures. HF elimination following the retro-Bergman ring-opening **16** is likely a minor/negligible contribution because the reagent 5-anion must be significantly less abundant than others.

The *m*-pyridinide anion yields specific products of HC_4^- and HC_4^-(HF) upon high-energy CID, the latter product of which corresponds to elimination of HCN. We attribute these products to dissociation of **7** via **TS3**, the primary product specific to the *m*-anion CID. If **7** decomposes promptly in the presence of HF, i.e., $[\mathbf{7} + HF]^- \rightarrow [HCN + HF + HC_4^-]$, both HC_4^- and HC_4^-(HF) could result. Another possibility for the HCN loss is retro-Diels–Alder decomposition of **1** to **5**. This mechanism is unlikely, however, because a similar retro-Diels–Alder path for the *o*-anion would form **13** then HCCH and NC_3^-(HF) at *m*/*z* 70. No species at *m*/*z* 70 was observed from CID of the *o*-anion. The retro-Diels–Alder decompositions are obviously very high-energy processes. This argument also rules out a direct electrocyclic mechanism for the CID of fluoropyridinide anions without retention of the ring structure. In this mechanism, for example, the *m*-fluoropyridinide-4-anion (Fig. 5) would dissociate directly to the high-energy retro-Diels–Alder complex **5**. Decomposition of **12** via **TS8** may also release HCN within the dissociation complex, but this will lead to a more stable product pair $HC_4H + CN^-$ (as above). Further, this scheme is common to *o*- and *m*- anions and is instead a plausible mechanism for the production of CN^- as observed. Formation of other fragment product anions C_3N^- and HC_2^- is also rationalized by the calculated energy diagrams. Direct (for *m*-anion) and indirect (for *o*-anion) dissociations of **9** via **TS5** lead to $NCCC^- + HCCH$ (lower energy) and $NCCCH + HC_2^-$ (higher energy). The $[HC_2^-]/[NCCC^-]$ ratio increases at higher collision energies, which is also consistent with the predicted energetics.

5.3. CID mechanism of 2,6-difluoropyridinide anion

Fig. 10 shows CID schemes for the 2,6-difluoropyridinide anions. The 3-anion (≡0 kJ mol^{-1}) could initially form [fluoropyridyne + F^-] intermediates with 2-fluoro-5,6-didehydropyridine **26** and/or 2-fluoro-3,6-didehydropyridine **27**. Following a crossover transition state (not calculated) and proton abstraction, the intermediate **26** generates fluoropyridynide anions **30** and/or **31**. The crossover barrier is expected to be low in energy compared to **TS2** because of charge withdrawal by the ring fluorine atom, which would reduce the repulsive π-electron density above and below the ring. The intermediate **27** may form **30** and/or **32**, but the *para*-pyridyne in **27** could also undergo facile decomposition to **28** in a retro-Bergman fashion. Site-specific deprotonation enthalpies for **28**, i.e., $FC{\equiv}CCH^{(1)}{=}CH^{(2)}C{\equiv}N$ are calculated at MP4(SDQ)/6-31 + G(d)//B3LYP/6-311++G(d,p) to be $\Delta_{acid}H_{298} = 1452$ and 1529 kJ mol^{-1} for $H^{(1)}$ and $H^{(2)}$, respectively. F^- deprotonation of $H^{(2)}$ yields an anion of similar (Z) structure, whereas $H^{(1)}$

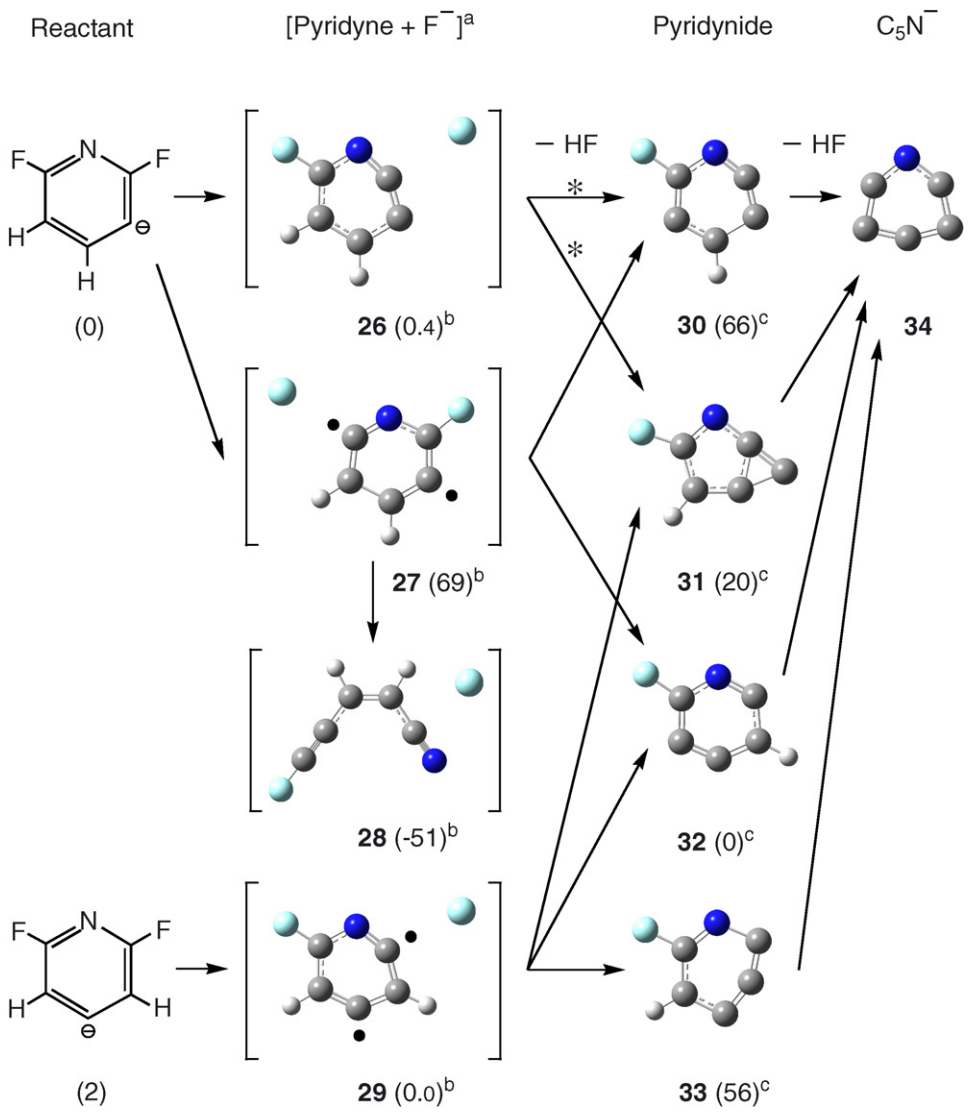

Fig. 10. Relative energies $\Delta_{298}H$ (electronic + ZEP + thermal correction) in kJ mol^{-1} calculated for the decomposition of 2,6-difluoropyridinide anions at MP4(SDQ)/6-31 + G(d)//B3LYP/6-311++G(d,p). [a]Energies for isolated neutral C_5NH_2F structures are shown; [b]Energies relative to **29**. [c]Energies relative to **32**. The asterisks indicate pathways requiring passage over a crossover transition state.

deprotonation results in a significant conformational change to form a bent skeleton at the $CH^{(2)}$ position. This is the only mechanism for HF elimination of the 2,6-difluoropyridinide anion *without* forming the fluoropyridynide structures. The slightly less stable 4-anion (2 kJ mol^{-1}) initially forms an intermediate with 2-fluoro-4,6-didehydropyridine **29**, which leads to fluoropyridynides **31**, **32**, and/or **33**. With increased internal excitation of the reactants, the nascent fluoropyridynide anions could sequentially lose the second HF molecule to produce the tetradehydropyridynide anion **34**.

Ring-opened transition states and products for the fluoropyridynide anions are summarized in Fig. 11. Adiabatic electron binding energies (electronic + ZPE) are calculated at B3LYP/6-311++G(d,p) to be 2.70 (**30**), 2.05 (**31**), 2.61 (**32**), and 1.91 eV (**33**). The mechanisms for ring cleavage are essentially the same as those for the non-fluorinated pyridynides (Fig. 7) and the heights of the transition states are also similar. If **30**, **32**, or **33** ring-opens, there is no feasible mechanism for the respective chain structures **35**, **36**, or **37** to lose the second HF molecule. The fluoropyridynide **31** is different, however. It can be seen that the fluorine atom is fairly loose at **TS11**. Following the transition state it is shown that the fluoride species abstracts the adjacent hydrogen to initially form a T-shaped NCCCCC$^-$(HF) structure, which then rearranges to the more stable linear NCCCCC$^-$(HF) complex (**39** in Figs. 12 and 13, see below) before dissociating to NCCCCC$^-$ (**38**) + HF. Overall, this provides the only mechanism for elimination of the second HF *without* forming tetradehydropyridynide **34**.

Figs. 12 and 13 show the potential energy diagrams for CIDs of the 3-anion and 4-anion of difluoropyridine, respectively. Similar to monofluoropyridinides, the energy diagrams are consistent with the experimental observation that HF elimination is the lowest dissociation channel. At MP4(SDQ)/6-31 + G(d)//B3LYP/6-311++G(d,p) the relative energies are 336 and 405 kJ mol^{-1} for the productions of **26** + F$^-$ and **27** + F$^-$ from the 3-anion, respectively (in the scale of Fig. 12), and

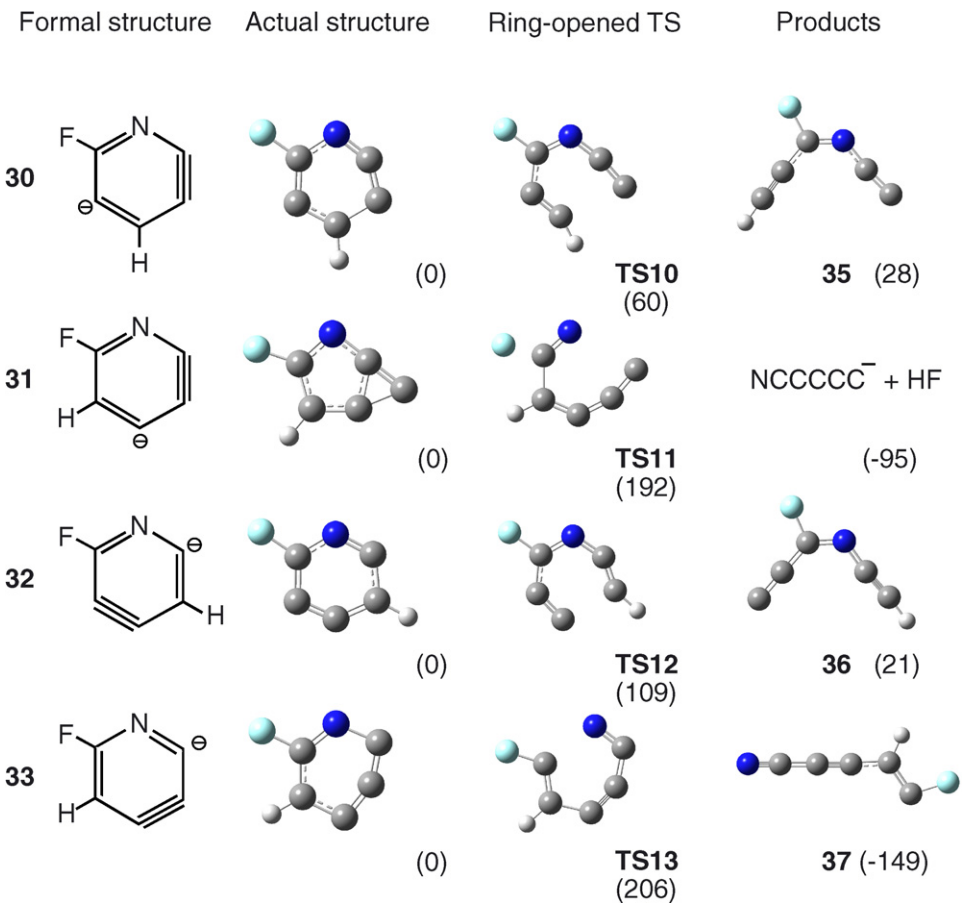

Fig. 11. Relative energies $\Delta_{298}H$ (electronic + ZEP + thermal correction) in kJ mol^{-1} calculated for ring-opening of the fluoropyridynide anions at MP4(SDQ)/6-31 + G(d)//B3LYP/6-311++G(d,p). All energies are relative to each of the fluoropyridinide structures.

335 kJ mol^{-1} for the production of **29** + F$^-$ from the 4-anion (in the scale of Fig. 13). Formation of fluoropyridynide anions **30**–**33** are all lower in energy than the F$^-$ elimination channels. Further, the reaction enthalpies for F$^-$ elimination of difluoropyridinide anions are considerably greater than those for *o*- and *m*-pyridinides. This is also consistent with the experiments that the difluoropyridinide produces a relatively small amount of F$^-$ compared to the monofluoropyridinides. In the CID of the 3-anion, the nascent *para*-pyridyne species **27** may undergo a retro-Bergman ring-opening to form **28** within the complex. Chain anions that could result from HF elimination

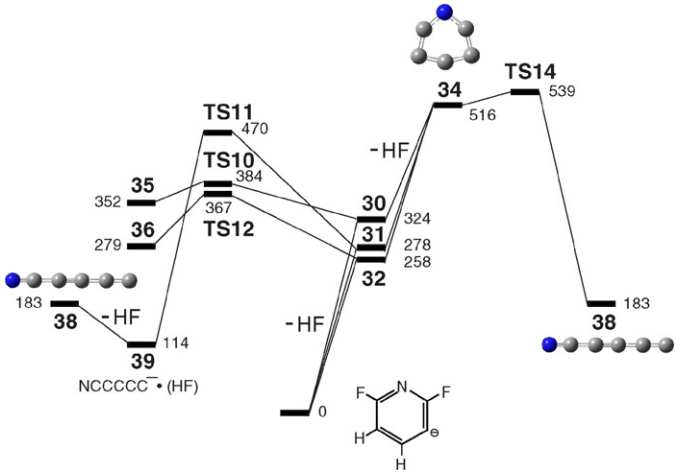

Fig. 12. Reaction energy diagram for the decomposition of 2,6-difluoropyridinide-3-anion. The relative energies $\Delta_{298}H$ (electronic + ZPE + thermal correction) are calculated at MP4(SDQ)/6-31+G(d)//B3LYP/6-311++G(d,p) and shown in kJ mol^{-1}.

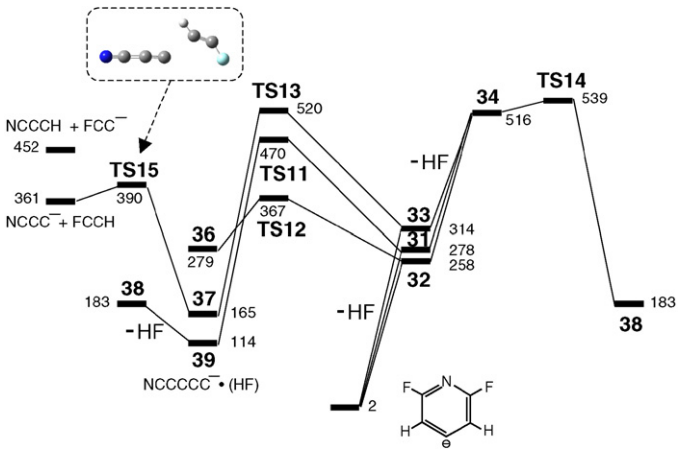

Fig. 13. Reaction energy diagram for the decomposition of 2,6-difluoropyridinide-4-anion. The relative energies $\Delta_{298}H$ (electronic + ZPE + thermal correction) are calculated at MP4(SDQ)/6-31+G(d)//B3LYP/6-311++G(d,p) and shown in kJ mol^{-1}.

of **28**, however, have no plausible mechanism to lose the second HF molecule. The observation of successive HF elimination strongly suggests that the retro-Bergman mechanism is minor and fluoropyridynide structures **30–33** are largely intact following elimination of the first HF molecule.

The ring-intact C_5N^- species **34** following elimination of the second HF molecule, however, is high in energy compared to the ring-opening barriers **TS10–TS12**; only **TS13** is comparable in energy to **34**. Although it is possible to form **34** at high levels of collisional excitation, the **TS14** barrier to ring-opening is sufficiently low that **34** will most likely dissociate to the linear $NCCCCC^-$ structure **38**. It is known empirically that ions with dissociation barriers of 15 kcal mol^{-1} (63 kJ mol^{-1}) or less do not survive the high-pressure flow tube at room temperature. A more plausible mechanism for the elimination of the second HF would be dissociation of **31** via **TS11** (as above), producing the linear $NCCCCC^-$ anion.

C_3N^- is a major fragmentation product from CID of the difluoropyridinides. A likely mechanism is ring-opening of **33** via **TS13** to form **37**, which further dissociates via **TS15** to C_3N^- and FCCH (Fig. 13). At higher collision energies **37** may also competitively yield the higher-energy product pair $HC_3N + FC_2^-$. Unlike CID processes of *o*- and *m*-fluoropyridinides (via **TS5**), HC_2^- will not form. This mechanism is consistent with the observed distributions of the CID fragments. Analogous to the ring-opening of **12**, it is speculated that ring-opening of **31** may also serve as a source for the observed product CN^- (+FC_4H) in addition to HC_4^- (+FCN) at high collision energies; the latter product pair is 64 kJ mol^{-1} higher in energy at MP4(SDQ)/6-31 + G(d)//B3LYP/6-311++G(d,p).

5.4. Structures and energetics of C_5N^- anion

Fig. 14 depicts the detailed $[C_5, N]^-$ potential energy diagram with the bond parameters for the C_5N^- anion **34** shown in the inset. At both MP4(SDQ)/6-31 + G(d)//B3LYP/6-311 + +G(d,p) and MP4(SDQ)/6-31 + G(d)//MP2/6-31+G(d) levels of theory, the bell structure **34** connects to a spade-shaped isomer **40** via a low energy barrier **TS16** (635 *i* cm^{-1} at MP2/6-31 + G(d)). All attempts to locate a ring-opened transition state from the spade anion resulted in rearrangement back to the more stable bell anion. The ring-intact anion **34** is a stable structure at MP4//B3LYP but it is only stable electronically at MP4//MP2. At the B3LYP/6-311++G(d,p) level of theory, adiabatic electron binding energies of the ring-intact and chain C_5N^- anions are 2.71 and 4.39 eV, respectively. As **34** ring-opens metastably to the C_5N^- chain anion **38** via **TS14** (612 *i* cm^{-1} at MP2/6-31 + G(d)), it releases approximately 80 kcal mol^{-1} (340 kJ mol^{-1}) of energy. The C_5N^- ring anion is thus a highly energetic species, although it is also susceptible to decomposition due to the low kinetic barrier. The corresponding non-aza substituted C_6H^- bell anion releases 40–50 kcal mol^{-1} (170–210 kJ mol^{-1}) of energy upon ring-opening to the linear C_6H^- structure (Kato et al., unpublished results), while it is significantly more stable against metastable decomposition with the kinetic barrier of 20–30 kcal mol^{-1} (80–120 kJ mol^{-1}).

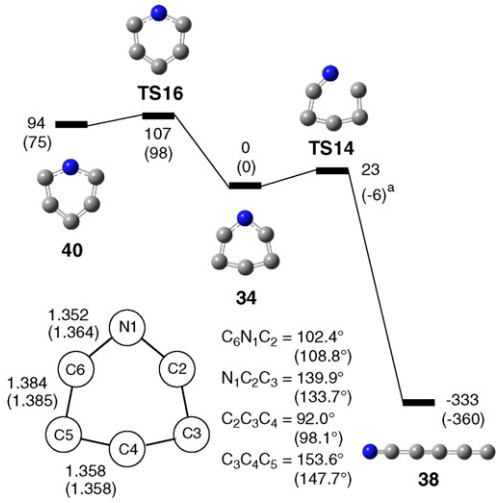

Fig. 14. Relative energies (ΔH_{298} in kcal mol^{-1}) and structures on the C_5N^- potential energy surface (electronic energy + ZPE + thermal correction) calculated at MP4(SDQ)/6-31 + G(d)//B3LYP/6-311++G(d,p). Relative energies at MP4(SDQ)/6-31 + G(d)//MP2/6-31 + G(d) are also indicated in parentheses ([a]the electronic energy is higher than the bell structure by 2.5 kJ mol^{-1}). Geometry parameters for **34** (C_{2v}), optimized with B3LYP/6-311++G(d,p) or MP2/6-31 + G(d) in parentheses, are shown by the inset (bond lengths in units of Å).

Pentazolide anion N_5^- has been generated in the gas phase [7]. It also displays metastable decomposition with the calculated barrier [40] of ca. 28 kcal mol^{-1} (120 kJ mol^{-1}), generating approximately 14 kcal mol^{-1} (60 kJ mol^{-1}) of energy upon forming N_3^- and N_2.

6. Conclusions

Collision-induced dissociations of *o*-fluoro, *m*-fluoro, and 2,6-difluoropyridinide anions proceed primarily via molecular eliminations of HF, which is similar to the CID of fluorophenyl anions. Elimination of F^- is a minor process for all reactant anions. The CID energy dependences of the product distributions are compared with the calculated reaction energy diagrams. The results strongly suggest that the produced anions are ring-intact pyridynide structures when generated at low collision energies. Transition states and products have also been identified computationally for ring-opening of the pyridynide anions, which occurs at higher collision energies. Observed distributions of fragmentation products are totally consistent with theory, substantiating the proposed CID mechanisms. For the CID of the difluoropyridinide anion, successive elimination of two HF molecules is observed, again similar to the CID of difluorophenide anions. The produced C_5N^- anion is most likely a chain structure $NCCCCC^-$ and not the tetradehydropyridinide anion under experimental conditions. The ring-intact C_5N^- pyridynide, however, is computationally characterized as a metastable structure with a kinetic barrier of about 5 kcal mol^{-1} (20 kJ mol^{-1}) and releases approximately 80 kcal mol^{-1} (340 kJ mol^{-1}) of energy upon ring-opening to the chain anion. As such, this is a high energy density species that is even more energetic than the pentazolide anion of current energetic interest.

Acknowledgements

This work was supported by the Air Force Office of Scientific Research and by the National Science Foundation (CHE-0349937). The authors are thankful to Prof. Charles H. DePuy for motivating them into the project and also to Prof. Scott Gronert for conducting initial experiments.

References

[1] R.W. Hoffmann, Dehydrobenzene and Cycloalkynes, Academic Press, New York, 1967.
[2] J. Cioslowski, A. Szarecka, D. Moncrieff, Mol. Phys. 101 (2003) 839.
[3] J. Fabian, E. Lewars, Can. J. Chem. 82 (2004) 50.
[4] R.J. Bartlett, Chem. Ind. (2000) 140.
[5] V. Benin, P. Kaszynski, J.G. Radziszewski, J. Org. Chem. 67 (2002) 1354.
[6] R.N. Butler, J.C. Stephens, L.A. Burke, Chem. Commun. (2003) 1016.
[7] A. Vij, J.G. Pavlovich, W.W. Wilson, V. Vij, K.O. Christe, Angew. Chem. Int. Ed. 41 (2002) 3051.
[8] J. Kramer, R.S. Berry, J. Am. Chem. Soc. 94 (1972) 8336.
[9] H.-H. Nam, G.E. Leroi, J. Am. Chem. Soc. 110 (1988) 4096.
[10] H.-H. Nam, G.E. Leroi, Tetrahedron Lett. 31 (1990) 4837.
[11] L. Radom, R.H. Nobes, D.J. Underwood, W.-K. Li, Pure Appl. Chem. 58 (1986) 75.
[12] A.P. Bruins, A.J. Ferrer-Correia, A.G. Harrison, K.R. Jennings, R.K. Mitchum, Adv. Mass Spectrom. 7A (1978) 355.
[13] Y. Guo, J.J. Grabowski, Int. J. Mass Spectrom. Ion Processes 117 (1992) 299.
[14] Y. Guo, J.J. Grabowski, J. Am. Chem. Soc. 113 (1991) 5923.
[15] J. Lee, J.J. Grabowski, Chem. Rev. 92 (1992) 1611.
[16] S. Gronert, C.H. DePuy, J. Am. Chem. Soc. 111 (1989) 9253.
[17] P.H. Tomperi, H.E.K. Matimba, S. Ingemann, N.M.M. Nibbering, Rapid Commun. Mass Spectrom. 7 (1993) 749.
[18] P.G. Wenthold, J.A. Paulino, R.R. Squires, J. Am. Chem. Soc. 113 (1991) 7414.
[19] H.V. Linnert, J.M. Riveros, J. Chem. Soc., Chem. Commun. (1993) 48.
[20] H.V. Linnert, J.M. Riveros, Int. J. Mass Spectrom. Ion Processes 140 (1994) 163.
[21] V.M. Bierbaum, in: M.L. Gross, R. Caprioli (Eds.), Encyclopedia of Mass Spectrometry, vol. 1, Theory and Ion Chemistry., Elsevier, Amsterdam, 2003, p. 276.
[22] S. Kato, J. Mass Spectrom. Soc. Jpn. 53 (2005) 183.
[23] J.M. Van Doren, S.E. Barlow, C.H. DePuy, V.M. Bierbaum, Int. J. Mass Spectrom. Ion Processes 81 (1987) 85.
[24] S.J. Blanksby, S. Kato, V.M. Bierbaum, G.B. Ellison, Aust. J. Chem. 56 (2003) 459.
[25] S. Kato, R. Gareyev, C.H. DePuy, V.M. Bierbaum, J. Am. Chem. Soc. 120 (1998) 5033.
[26] M.J. Frisch, G.W. Trucks, H.B. Schlegel, G.E. Scuseria, M.A. Robb, J.R. Cheeseman, J.A. Montgomery, T. Vreven Jr., K.N. Kudin, J.C. Burant, J.M. Millam, S.S. Iyengar, J. Tomasi, V. Barone, B. Mennucci, M. Cossi, G. Scalmani, N. Rega, G.A. Petersson, H. Nakatsuji, M. Hada, M. Ehara, K. Toyota, R. Fukuda, J. Hasegawa, M. Ishida, T. Nakajima, Y. Honda, O. Kitao, H. Nakai, M. Klene, X. Li, J.E. Knox, H.P. Hratchian, J.B. Cross, C. Adamo, J. Jaramillo, R. Gomperts, R.E. Stratmann, O. Yazyev, A.J. Austin, R. Cammi, C. Pomelli, J.W. Ochterski, P.Y. Ayala, K. Morokuma, G.A. Voth, P. Salvador, J.J. Dannenberg, V.G. Zakrzewski, S. Dapprich, A.D. Daniels, M.C. Strain, O. Farkas, D.K. Malick, A.D. Rabuck, K. Raghavachari, J.B. Foresman, J.V. Ortiz, Q. Cui, A.G. Baboul, S. Clifford, J. Cioslowski, B.B. Stefanov, G. Liu, A. Liashenko, P. Piskorz, I. Komaromi, R.L. Martin, D.J. Fox, T. Keith, M.A. Al-Laham, C.Y. Peng, A. Nanayakkara, M. Challacombe, P.M.W. Gill, B. Johnson, W. Chen, M.W. Wong, C. Gonzalez, J.A. Pople, Gaussian 03, Revision B.05, Gaussian Inc., Pittsburgh, PA, 2003.
[27] C. Gonzalez, H.B. Schlegel, J. Chem. Phys. 90 (1989) 2154.
[28] C. Gonzalez, H.B. Schlegel, J. Phys. Chem. 94 (1990) 5523.
[29] J.B. Foresman, Æ. Frisch, Exploring Chemistry with Electronic Structure Methods, Gaussian Inc., Pittsburgh, 1996.
[30] R. Lindh, T.J. Lee, A. Bernhardsson, B.J. Persson, G. Karlström, J. Am. Chem. Soc. 117 (1995) 7186.
[31] P.J. Linstrom, W.G. Mallard (Eds.), NIST Chemistry WebBook, NIST Standard Reference Database Number 69, National Institute of Standards and Technology, Gaithersburg MD, 2005 http://webbook.nist.gov.
[32] S. Sharma, J.K. Lee, J. Org. Chem. 67 (2002) 8360.
[33] C.H. DePuy, S. Kato, in: M.L. Gross, R. Caprioli (Eds.), Encyclopedia of Mass Spectrometry, Elsevier, Amsterdam, 2003, p. 670.
[34] S. Kato, C.H. DePuy, S. Gronert, V.M. Bierbaum, J. Am. Soc. Mass Spectrom. 10 (1999) 840.
[35] X. Zhang, A.T. Maccarone, M.R. Nimlos, S. Kato, V.M. Bierbaum, G.B. Ellison, B. Ruscic, A.C. Simmonett, W.D. Allen, H.F. Schaefer, J. Chem. Phys. 126 (2007) 044312.
[36] L.V. Moskaleva, L.K. Madden, M.C. Lin, Phys. Chem. Chem. Phys. 1 (1999) 3967.
[37] W.M. David, S.M. Kerwin, J. Am. Chem. Soc. 119 (1997) 1464.
[38] J. Hoffner, M.J. Schottelius, D. Feichtinger, P. Chen, J. Am. Chem. Soc. 120 (1998) 376.
[39] L. Sun, K. Song, W.L. Hase, Science 296 (2002) 875.
[40] M.T. Nguyen, T.-K. Ha, Chem. Phys. Lett. 335 (2001) 311.